

Ateneo de Manila University

Archium Ateneo

Chemistry Faculty Publications

Chemistry Department

10-2020

Bentonite Reinforced Chitosan Scaffold: Effect of Bentonite Exfoliation on Scaffold Properties

Soma Chakraborty

Cristine Joy M. Pimentel

Follow this and additional works at: <https://archium.ateneo.edu/chemistry-faculty-pubs>



Part of the [Environmental Chemistry Commons](#)

Bentonite Reinforced Chitosan Scaffold: Effect of Bentonite Exfoliation on Scaffold Properties

Soma Chakraborty* and Cristine Joy M. Pimentel

Department of Chemistry, School of Science and Engineering
Ateneo de Manila University, Loyola Heights, Quezon City 1108 Philippines

Chitosan is under investigation as a biodegradable scaffolding material for tissue engineering. Crosslinked chitosan alone cannot form a self-supporting scaffold; hence, it needs reinforcement. The group reported the fabrication of chitosan scaffolds reinforced by exfoliated (E) and non-exfoliated or pristine (P) bentonite and compared their properties. Scaffolds were fabricated through the freeze-drying technique. Bentonite was exfoliated by allowing it to swell in water for a certain time interval. X-ray powder diffraction (XRD) profile showed that swelling reduced the crystallinity of bentonite. Both types of bentonite dispersed well in the chitosan matrix and imparted structural stability to the scaffolds. Scaffolds had interconnected pores; apparent porosity of scaffold with E-bentonite was higher than of scaffold with P-bentonite. The scaffolds swelled almost 35% in 3 d without losing structural integrity. The scaffolds could be compressed to 50% of their original height. The compression modulus of the scaffold with E-bentonite was higher than that of the P-bentonite scaffold.

Keywords: bentonite, chitosan, reinforcement, scaffold

INTRODUCTION

Chitosan is a natural nontoxic polysaccharide with a wide scope of biomedical applications. It has antibacterial, hemocompatibility, and cytocompatibility properties; it likewise aids in the enhancement of cell adhesion, proliferation, osteoblast differentiation, and mineralization (Balagangadharan *et al.* 2017; Sahranavard *et al.* 2017). It has the inherent strength to get molded as gel, film, and scaffold. These appealing properties make chitosan a promising material for tissue engineering. Chitosan, in combination with other biopolymers, has been extensively investigated as a scaffold (Levengood and Zhang 2014; Soundarya *et al.* 2018; Ahmed *et al.* 2018; Si *et al.* 2019).

To broaden the application range of chitosan, the mechanical strength of chitosan has been enhanced by reinforcing it using inorganic fillers. Improvement in elastic modulus of chitosan scaffold upon the addition

of hydroxyapatite has been studied by Teng *et al.* (2009). Incorporation of nano-hydroxyapatite in chitosan to improve the compression strength, cell proliferation, and cell attachment of osteoblasts has been cited (Thein-Han and Misra 2009). Similarly benefits of using multiwalled carbon nanotubes (Fan *et al.* 2012), graphene (Mittal *et al.* 2017), graphene oxide (Francolini *et al.* 2019), and silver nanoparticles (Mohamed and Madian 2020) to increase the tensile strength of chitosan have been documented.

Recently, the use of bentonite as a filler for the chitosan matrix is also under investigation. Bentonite is a synthetic aluminosilicate nano-platelet having a layered structure, which not only serves as a reinforcing agent for polymers but can also impart antimicrobial behavior. Furthermore, it is non-toxic, of low cost, readily available, and with high cation-exchange capacity. Hence, it serves as a filler for composites from synthetic (Kotal and Bhowmick 2015; Alghamdi *et al.* 2019; Serge *et al.* 2019) and natural polymers (Gong *et al.* 2018; Kong *et al.* 2019; Oussalah *et*

*Corresponding Authors: schakraborty@ateneo.edu

al. 2019). Its apatite forming ability (Cao *et al.* 2015; Ali *et al.* 2019) and ability to induce osteogenic differentiation in human mesenchymal stem cell without using any growth factors (Gaharwar *et al.* 2014) makes it a potential reinforcing agent for bone regeneration scaffolds.

So far, bentonite has been integrated into chitosan composites mainly for water treatment (Haseena *et al.* 2016; Motshekga and Ray 2017; Dehghani *et al.* 2018; Jimtaison and Sarakonsri 2019; Wang *et al.* 2019; Xu *et al.* 2020), wound healing (Devi and Dutta 2017; Shanmugapriya *et al.* 2018), and enzyme immobilization (Benucci *et al.* 2018; Kaushal *et al.* 2018; Tavernini *et al.* 2020).

There are few studies illustrating the scaffold forming ability of chitosan in combination with other polymers and reinforced by bentonite (Ali *et al.* 2019). However, there is no report of using chitosan alone with bentonite for the fabrication of scaffold. Hence, this study explored the potential of chitosan to form a scaffold reinforced by bentonite. Our group reported the fabrication of three-dimensional (3D) chitosan scaffold reinforced with E- and P-bentonite through the freeze-drying technique. We exfoliated bentonite solely by dispersing it in water under sonication. Furthermore, we compared the properties of these two types of scaffolds.

Chitosan forms a polyelectrolyte complex with bentonite due to the strong electrostatic interaction between polycationic chitosan and negatively charged bentonite (Devi and Dutta 2017; Savitri and Budhyantoro 2017); thus, it can be hypothesized that bentonite can serve as an effective reinforcing agent for chitosan scaffold. Bentonite, owing to its electrostatic attraction for chitosan, is expected to disperse easily in chitosan matrix unlike other inorganic fillers (Francolini *et al.* 2019; Mohamed and Madian 2020). It can also be anticipated that bentonite will not have a significant impact on the tensile strength of the matrix – unlike other high strength fillers such as carbon nanotubes and graphene – but will improve the compressive strength of the system, which is critical for scaffold formation. High strength fillers improve the tensile strength but compromise with the compressive strength (Mohamed and Madian 2020).

MATERIALS AND METHODS

Materials

Medium molecular weight chitosan (catalog # 448877), glutaraldehyde (catalog # G6257, Grade II, 25% in H₂O), acetic acid (catalog # 695092, glacial, ReagentPlus®, ≥ 99%), and bentonite (catalog # 285234, montmorillonite)

were purchased from Sigma Aldrich, USA. Water used for the study was distilled in the Chemistry Department of Ateneo de Manila University, Philippines.

Exfoliation of Bentonite

0.1 g of bentonite was dispersed in 10 mL of deionized water and it was sonicated for 6 h and was left at room temperature for 3 d. This dispersion was freeze-dried for further use.

Chitosan Bentonite Scaffold

Chitosan (0.1 g) was dissolved in 10 mL of 2% (v/v) acetic acid. In a separate beaker, 0.1 g of bentonite was dispersed in 10 mL of deionized water by stirring the system for 4 h at room temperature. The chitosan solution and the bentonite dispersion were mixed together in a beaker and stirred for 4 h, followed by the addition of 2.5 mL of 1% (v/v) glutaraldehyde solution. The reaction mixture was stirred further for 4h, frozen in liquid N₂, and then freeze-dried for 72 h at –80°C and 3 Pa using the Eyela Freeze dryer FDU-2200.

The porosity of the scaffolds was quantified using the ethanol displacement test, as reported by Xu *et al.* (2012). Absolute ethanol with a density of 0.785 g/mL was used as a displacement liquid, as ethanol easily penetrate the scaffold without interacting with it. Scaffolds were cut into a cylindrical shape using a thin blade cutter and their volume (V_{scaffold}) was calculated by measuring the diameter and the thickness using a ruler. The weight of each sample (W_0) was recorded and placed in a vial containing ethanol. The vials were sonicated for 30 min to allow the ethanol to fully impregnate the scaffolds and then the wet weights of the scaffolds (W) were measured. The following equation was used to calculate apparent porosity of the scaffolds:

$$\text{Apparent Porosity} = \frac{(w - w_0)}{(\rho_{\text{EtOH}})(V_{\text{scaffold}})} \times 100 \quad (1)$$

To evaluate the extent of swelling of the scaffolds, 0.10 g of the scaffold was immersed in 10 mL of pH 7.4 buffer solution in a vial for a certain time interval. Then, the scaffolds were collected from the vials, placed on a paper towel, and gently patted with another paper towel very briefly; the wet paper towel was discarded thereafter. It was again patted with another paper towel in similar way. The process was repeated five to six times until no trace of water was detected on the paper. The percent swelling values of the systems were computed using Equation 2, where w_0 and w are the weights of the scaffold before and after immersion in the buffer solution, respectively:

$$\text{Swelling \%} = \frac{w - w_0}{w_0} \times 100 \quad (2)$$

RESULTS AND DISCUSSION

Exfoliated and Pristine Bentonite

Bentonite was dispersed in deionized water under sonication to disrupt its crystalline structure in order to enhance its interaction with chitosan. There was no difference in physical appearance between E- and P-bentonite. However, the difference in the XRD profile of E-bentonite and P-bentonite was observed, which is discussed in the following section.

XRD and % Crystallinity of Bentonite

The crystallinity of exfoliation and pristine bentonite was determined using the Rigaku Ultima IV X-ray diffractometer. The scan rate was 5° per minute at a wavelength of 1.54 Å (Cu-K α), and the 2 θ range was from 5–85°. The crystallinity of the peaks was calculated using the OriginPro 2020 software.

The XRD profiles of E- and P-bentonite are shown in **Figure 1**. Both of them have peaks representing montmorillonite, sepiolite, and quartz. In the case of E-bentonite, the (001) characteristic peak of montmorillonite at 2 θ < 10° was broader and weaker than that of P-bentonite, indicating the delamination of the stacked layers after exfoliation. A similar observation was made by Ma *et al.* (2016) and Wang *et al.* (2020).

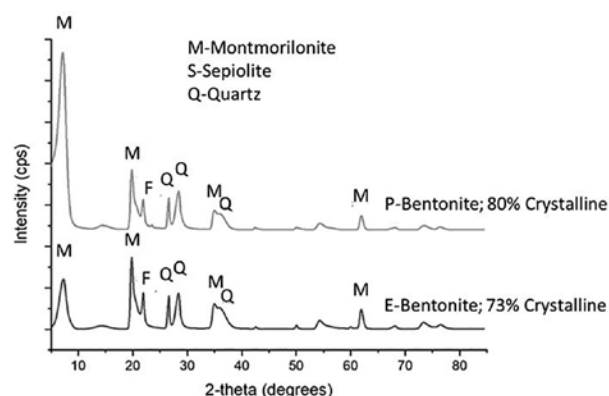


Figure 1. XRD profile of E- and P-bentonite.

% crystallinity as calculated from the peak areas also revealed that prolonged dispersion in water reduced the overall crystallinity of bentonite, most probably due to shifting in its clay platelets of bentonite as reported elsewhere (Diman and Wijeyesekera 2008). Thus, it can be assumed that bentonite got exfoliated merely by dispersing it in water for a long time interval.

Physical Appearance of the Scaffolds

3D structures of the scaffolds are shown in **Figure 2**. The freeze-dried scaffolds fabricated using E- and P-bentonite

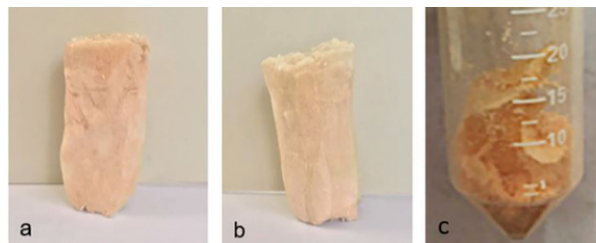


Figure 2. Physical appearance of the scaffolds with (a) E-bentonite, (b) P-bentonite, and (c) chitosan only.

was light yellow in color, self-supporting with sponge-like texture. The scaffold that was fabricated with chitosan only, crumpled after freeze-drying, implying that bentonite serves as the reinforcing agent for chitosan scaffold. Hence, the chitosan scaffold without bentonite was not studied further.

FTIR Spectrum

Shimadzu IR Affinity-1 FTIR8400S was used to obtain the FTIR spectra of chitosan, bentonite, and the scaffolds. A small amount of powdered sample was ground with dried KBr powder and was pressed mechanically using the Shimadzu KBr tablet die to form a disc. For each sample, a 40-scan interferogram at 4000–400 cm⁻¹ was collected in terms of percent transmittance (%T).

Figure 3 shows the FTIR spectra of chitosan, E-bentonite, and E-bentonite reinforced scaffold. In the FTIR spectrum of chitosan, a broad band appears at 3400 cm⁻¹ due to the overlapped stretching vibrations from the -NH₂ and -OH groups of chitosan. The peak at 1651 cm⁻¹ has been associated with the Schiff base formed from the reaction of chitosan and glutaraldehyde. The peak at 1562 cm⁻¹ is related to the vibrations of protonated amine groups of the chitosan chain and a peak at 1050 cm⁻¹ originates from the C-O group of chitosan. In the FTIR spectrum of

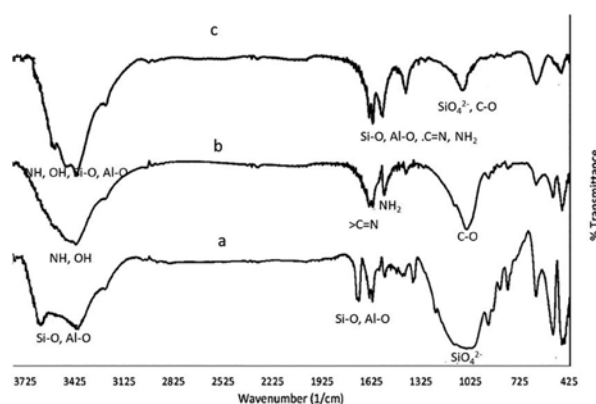


Figure 3. FTIR spectrum of a) E-bentonite, b) glutaraldehyde crosslinked chitosan, and c) E-bentonite reinforced chitosan scaffold.

E-bentonite, peaks at 3618–3439 cm^{-1} and at 1699–1631 cm^{-1} are due to the presence of Si-O and Al-O groups. The broad peak at 3400–3450 cm^{-1} is also attributed to the -OH linkages between the octahedral and tetrahedral layers of the silicate structure. A broad peak at 1000 cm^{-1} represents the SiO_4^{2-} of bentonite. All these characteristic peaks are likewise visible in the E-bentonite reinforced scaffold.

Scaffold Morphology

Morphology and interconnectivity of the scaffolds were studied using a scanning electron microscope (SEM). A portion of the scaffold was gently placed on the carbon tape without compressing it. The scaffolds were viewed using JSM-5310 SEM at 10 kV under different magnifications.

Figure 4 shows the SEM images of the scaffolds. It can be observed that the scaffolds with E- as well as P-bentonite showed interconnected porous morphology, which is desirable for cell growth and proliferation. No agglomeration of bentonite was detected in the porous scaffold, indicating that bentonite could get dispersed very well in chitosan matrix simply by stirring, whereas a study in past showed that it was challenging to disperse hydroxyapatite reinforcing agent in chitosan-carrageenan matrix scaffold as agglomerates hydroxyapatite was clearly visible in the scanning electron micrograph (Chakraborty *et al.* 2018). Strong electrostatic interaction between polycation cation and anionic bentonite might have facilitated efficient dispersion of bentonite in the chitosan matrix (Devi and Dutta 2017; Savitri and Budhyantoro 2017).

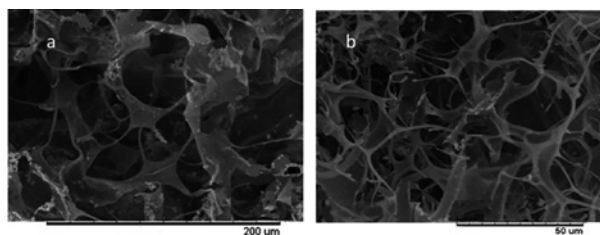


Figure 4. Scanning electron micrograph of (a) P-bentonite scaffold and (b) E-bentonite scaffold.

Scaffold Porosity

Scaffolds are required to be porous to facilitate the delivery of nutrition to the cells for their growth. The porosity of the scaffolds was quantified through the ethanol displacement test. Scaffold with P-bentonite showed $92.7 \pm 2.1\%$ porosity, which further enhanced to $97.3 \pm 1.8\%$ when E-bentonite was used. Experiments were performed in triplets.

The process of formation of a porous scaffold involves freezing the scaffolding materials followed by freeze-drying. Rapid freezing triggers the formation of solvent crystals, which sublime during freeze-drying leading to the formation of a porous structure. Pore size, volume, and morphology are dependent on various factors, including the nature of interaction with the solvent (Qian and Zhang 2011). An increase in specific surface and reduction of crystallinity in exfoliated might have favored the formation of more and/or bigger water crystals, eventually making the scaffold more porous. Enhancement of porosity of graphene oxide-chitosan scaffold by exfoliation of graphene oxide, owing to better interaction with water, has also been reported elsewhere (Francolini *et al.* 2019).

Swelling Behavior

The scaffolds are required to swell in moderation. They need to swell to allow cell growth; however, excessive swelling could lead to loss of their structural integrity. When the swelling behavior of the two types of scaffolds was compared at pH 7.4, as shown in Figure 5, it was observed that both types of scaffold swelled to almost 30% of their original weight in the first 6 h, beyond which no significant increase in swelling was observed. This suggests that the scaffolds undergo controlled swelling and, hence, have a better chance of maintaining structural integrity even after prolonged exposure to water or body fluid. It is surmised that the interaction between the chitosan-OH and $-\text{NH}_2$ with water regulates the swelling. Since the amount of chitosan is the same in both types of scaffolds, E- and P-bentonite scaffolds manifested comparable swelling.

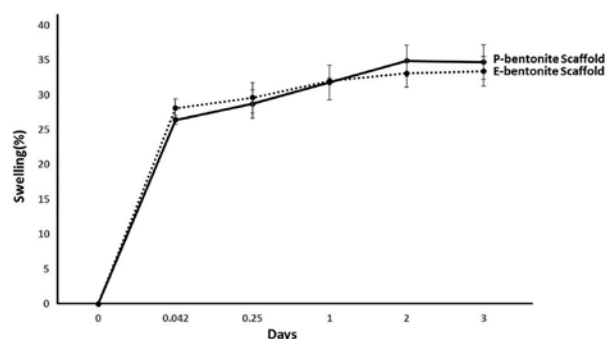


Figure 5. Swelling behavior of the scaffolds in pH 7.4 buffer. Each data point represents the average of three samples.

Compressibility

Compressibility of the scaffolds was measured using the Universal Testing Machine at a displacement rate of 10 mm/min with a maximum load of 500 N. The height and cross-sectional surface area of the scaffold were determined to be 30 cm and 15 cm, respectively, before

subjecting to compression load up to 50% of its original height. The compressive modulus was determined as the slope of the initial linear portion of the stress-strain curve.

The scaffolds are expected to undergo compression gradually as the bone tissues regenerate around them for healing purposes. As seen in **Figure 6**, the scaffolds could undergo compression upon application of load and regained the original form when the load was removed. When a maximum load of 500 N was applied, the E-bentonite scaffold got compressed from 30 to 28cm whereas P-bentonite scaffolds got compressed from 30 to 22 cm.

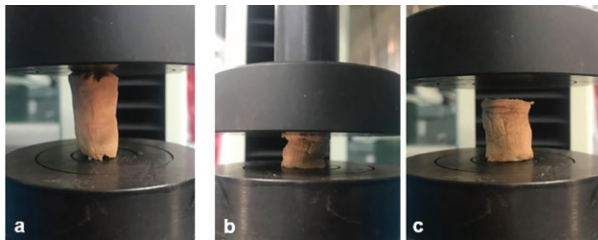


Figure 6. E-bentonite reinforced scaffold (a) before compression, (b) at 50% compression, and (c) after compression.

Figure 7 compares the compression stress-strain curve of the scaffolds. They were compressed to 50% of their original height under a maximum load of 500 N. The scaffold with E- and P- bentonite clay has a compressive modulus of 8300 Pa and 7900 Pa, respectively. Compressive strength varies with the stiffness of the material. It can be hypothesized that the disruption of the ordered structure of E-bentonite increased the surface contact between E-bentonite and chitosan, facilitating stronger interaction between the negatively charged bentonite plates and the polycationic chitosan. Consequently, it was made stiffer than the P-bentonite chitosan scaffold, which is reflected in its higher compressive modulus. Improvement in the compressive strength of clay brick by exfoliation (Niroumand *et al.* 2013) and the mortars by using exfoliated nano-scale metakaolin (Morsya *et al.* 2018) have been reported.

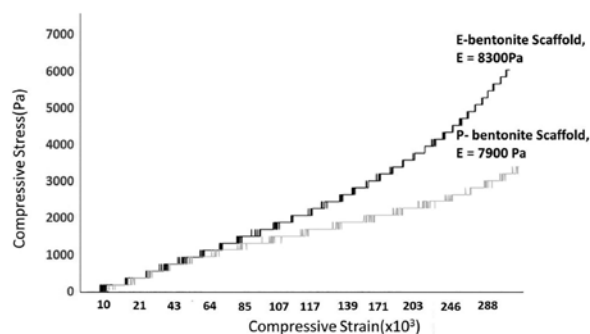


Figure 7. Stress-strain curve of the scaffolds reinforced with E- and P-bentonite.

SUMMARY AND CONCLUSIONS

Chitosan, a bioactive biodegradable polymer, is capable of serving as a scaffold for tissue engineering. However, it lacks the strength to form a self-supporting 3D structure. This study established that incorporation of bentonite in exfoliated and non-exfoliated form as a reinforcing filler aids chitosan to form a self-supporting scaffold and they can be fabricated through the freeze-drying method. Furthermore, the XRD profile of swelled bentonite revealed that dispersion of bentonite in water under sonication can likewise be an effective approach for exfoliation of bentonite, apart from using surfactant and other chemicals. Since no agglomeration of bentonite was detected in the SEM image of the scaffolds, it can be concluded that bentonite can be easily dispersed in the chitosan matrix. When kept immersed in pH 7.4 buffer, both types of scaffolds swelled in moderation without undergoing any structural disintegration. Thus, it can be hypothesized that the scaffold can act as a stable support system for cell growth under human physiological conditions. A comparison of apparent porosity showed that E-bentonite reinforced scaffolds were more porous than the P-bentonite reinforced scaffold; hence, it has the potential to promote better cell growth and adhesion. Compressive strength measurement demonstrated that E-bentonite reinforced scaffold has higher strength. Hence, it can be assumed that scaffold fabricated using E-bentonite will serve as a superior scaffold when compared with the P-bentonite reinforced scaffold.

Since chitosan is a biopolymer that is found in abundance, bentonite is a benign inexpensive reinforcing agent and the methodologies used for exfoliation of bentonite and fabrication of scaffold are very simple. Thus, this system can be explored further for the development of a benign, cost-effective scaffold for tissue engineering.

ACKNOWLEDGMENTS

The authors would like to acknowledge the Loyola School (Ateneo De Manila University) Faculty Grant for Scholarly Work for financial support. We would also like to express our gratitude to Dr. Jose Mario Diaz and Ms. Dorothy Claire G. Parungao for their assistance to perform the XRD experiments, and to Ms. Myelene Kaye Q. Vergara for performing some preliminary experiments.

REFERENCES

AHMED S, ALI AA, SHEIKH J. 2018. Controlled degradable chitosan/collagen composite scaffolds for

- application in nerve tissue regeneration. *Inter J Biol Macromol* 116: 849–862.
- ALGHAMDI MM, EL-ZAHHAR AA, EL NEMR A. 2019. Synthesis, characterization, and application of a novel polymeric-bentonite-magnetite composite resin for water softening. *Sep Purif Technol* 224(1): 356–365.
- ALI A, BANO S, POOJARY SS, KUMAR D, NEGI YS. 2019. Effect of incorporation of montmorillonite on Xylan/Chitosan conjugate scaffold. *Colloids and Surfaces. B, Biointerfaces* 180: 75–82.
- BALAGANGADHARAN K, DHIVYA S, SELVAM-URUGAN N. 2017. Chitosan based nanofibers in bone tissue engineering. *Int J Biol Macromol* 104: 1372–1382.
- BENUCCI I, LIBURDI K, CACCIOTTI I, LOMBARDELLI C, ESTI M. 2018. Chitosan/clay nanocomposite films as supports for enzyme immobilization: An innovative green approach for winemaking applications. *Food Hydrocolloids* 74: 124–131.
- CAO X, WANG J, LIU M, CHEN Y, CAO Y, YU X. 2015. Chitosan-collagen/organomontmorillonite scaffold for bone tissue engineering. *Front Mater Sci* 9: 405–412.
- CHAKRABORTY S, YATCO KAM. CHUA EKL, CHUA MT. 2018. Polyelectrolyte Complex of Chitosan and κ -Carrageenan as Potential Scaffold for Tissue Engineering *Sci Diliman* 30(2): 54–69.
- DEGHANI MH, ZAREI A, MCKAY G. 2018. Production and application of a treated bentonite–chitosan composite for the efficient removal of humic acid from aqueous solution. *Chem Eng Res Des* 140: 102–115.
- DEVI N, DUTTA J. 2017. Preparation and characterization of chitosan-bentonite nanocomposite films for wound healing application. *Inter J Biol Macromol* 104: 1897–1904.
- DIMAN SF, WIJESEKERA DC. 2008. Swelling Characteristics of Bentonite Clay Mats. *Proceedings of the AC&T*. p. 179–185.
- FAN J, SHI Z, GE Y, WANG Y, WANG J, YIN J. 2012. Mechanical reinforcement of chitosan using unzipped multiwalled carbon nanotube oxides. *Polymer* 53(2): 657–664.
- FRANCOLINI I, PERUGINI E, SILVESTRO I, LOPREIATO M, SCOTTO D’ABUSCO A, VALENTINI F, PLACIDI E, FABRIZIO ARCIPRETE F, MARTINELLI A, PIOZZI A. 2019. Graphene Oxide Oxygen Content Affects Physical and Biological Properties of Scaffolds Based on Chitosan/Graphene Oxide Conjugates. *Materials (Basel)* 12(7): 1142.
- GAHARWAR AK, MUKUNDAN S, KARACA E, DOLATSHAHI-PIROUZ A, PATEL A, RANGARAJAN K, MIHAILA SM, IVIGLIA G, ZHANG H, KHADEMHOSEINI A. 2014. Nanoclay-enriched poly(ϵ -caprolactone) electrospun scaffolds for osteogenic differentiation of human mesenchymal stem cells. *Tissue Eng Part A* 20: 2088–2101.
- GONG N, LIU Y, HUANG R. 2018. Simultaneous adsorption of Cu^{2+} and Acid fuchsin (AF) from aqueous solutions by CMC/bentonite composite. *Int J Biol Macromol* 115: 580–589.
- HASEENA PV, PADMAVATHY KS, ROHIT KRISHNAN P, MADHU G. 2016. Adsorption of Ammonium Nitrogen from Aqueous Systems Using Chitosan-Bentonite Film. *Composite Procedia Technology* 24: 733–740.
- JIMTAISONG A, SARA KONSRI T. 2019. Chitosan intercalated bentonite as natural adsorbent matrix for water-soluble sappanwood dye. *Int J Biol Macromol* 12915: 737–743.
- KAUSHAL J, SEEMA, SINGH G, ARYA SK. 2018. Immobilization of catalase onto chitosan and chitosan-bentonite complex: a comparative study *Biotechnology Reports* 18: e00258.
- KONG Y, WANG L, GE Y, SU H, LI Z. 2019. Lignin xanthate resin–bentonite clay composite as a highly effective and low-cost adsorbent for the removal of doxycycline hydrochloride antibiotic and mercury ions in water. *J Hazard Mater* 368: 33–41.
- KOTAL M, BHOWMICK AK. 2015. Polymer nanocomposites from modified clays: recent advances and challenges. *Prog Polym Sci* 51: 127–187.
- LEVENGOD SL, ZHANG M. 2014. A review on chitosan centred scaffolds and their applications in tissue engineering. *J Mater Chem B Biol Med* 2(21): 3161–3184.
- MA J, HUANG D, ZHANG W, ZOU J, KOMARNENI S. 2019. Nanocomposite of exfoliated bentonite/g- $\text{C}_3\text{N}_4/\text{Ag}_3\text{PO}_4$ for enhanced visible-light photocatalytic decomposition of Rhodamine B. *Chemosphere* 162: 269–276.
- MITTAL G, RHEE KY, PARK SJ, HUIM D. 2017. Generation of the pores on graphene surface and their reinforcement effects on the thermal and mechanical properties of chitosan-based composites. *Compos B: Eng* 114: 348–355.
- MOHAMED N, MADIAN NG. 2020. Evaluation of the mechanical, physical and antimicrobial properties of

- chitosan thin films doped with greenly synthesized silver nanoparticles. *Mater Today Commun* 25: 101372.
- MORSYA MS, SHOUKRY H, MOKHTAR MM, ALI AM, EL-KHODARYA SA. 2018. Facile production of nano-scale metakaolin: an investigation into its effect on compressive strength, pore structure and microstructural characteristics of mortar. *Constr Build Mater* 172: 243–250.
- MOTSHEKGA S, RAY SS. 2017. Highly efficient inactivation of bacteria found in drinking water using chitosan-bentonite composites: modelling and breakthrough curve analysis. *Water Res* 111: 213–223.
- NIROUMAND H, ZAIN MFM, ALHOSSEINI SN. 2013. The Influence of Nano-clays on Compressive Strength of Earth Bricks as Sustainable Materials. *Procedia – Social and Behavioral Sciences* 89: 862–865.
- OUSSALAHA, BOUKERROUIA, AICHOOR A, BRAHIM DJELLOULI B. 2019. Cationic and anionic dyes removal by low-cost hybrid alginate/natural bentonite composite beads: adsorption and reusability studies. *Int J Biol Macromol* 124: 854–862.
- QIAN L, ZHANG H. 2011. Controlled freezing and freeze drying: a versatile route for porous and micro/nano-structured materials. *J Chem Technol Biotechnol* 86: 172–184.
- SAHRANAVARD M, ZAMANIAN A, GHORBANI F, SHAHREZAEI MH. 2020. A critical review on three dimensional-printed chitosan hydrogels for development of tissue engineering. *Bioprinting* 17: e00063.
- SAVITRI E, BUDHYANTORO A. 2017. The effect of ratio chitosan-bentonite and processing time on the characterization of chitosan-bentonite composite. *Mater Sci Eng* 223: 012034.
- SERGE EJ, ALLA JP, BELIBI PD, MBADCAM KJ, FATHIMA NN. 2019. Clay/polymer nanocomposites as filler materials for leather. *J Clean Prod* 237: 117837.
- SHANMUGAPRIYA K, KIM H, SARAVANA PS, CHUN B-S, KAND H. 2018. Fabrication of multifunctional chitosan-based nanocomposite film with rapid healing and antibacterial effect for wound management. *Int J Biol Macromol* 118: 1713–1725.
- SI J, YANG Y, XING X, YANG F, SHAN P. 2019. Controlled degradable chitosan/collagen composite scaffolds for application in nerve tissue regeneration. *Polym Degrad Stab* 166: 73–85.
- SOUNDARYA PS, MENON HA, CHANDRAN VS, SELVAMURUGAN N. 2018. Bone tissue engineering: Scaffold preparation using chitosan and other biomaterials with different design and fabrication techniques. *Int J Biol Macromol* 119: 1228–1239.
- TAVERNINI L, OTTONE C, ILLANES A, WILSON L. 2020. Entrapment of enzyme aggregates in chitosan beads for aroma release in white wines. *Int J Biol Macromol* 1541: 1082–1090.
- TENG S-H, LEE E-J, YOON B-H, SHIN D-S, KIM H-E, OH J-S. 2009. Chitosan/nanohydroxyapatite composite membranes *via* dynamic filtration for guided bone regeneration. *J Biomed Mater Res Part A* 88: 569–580.
- THEIN-HAN WW, MISRA RDK. 2009. Biomimetic chitosan-nanohydroxyapatite composite scaffolds for bone tissue engineering. *Acta Biomaterialia* 5(4): 82–1197.
- WANG K, MA H, ZINCHENKO A. 2019. Hybrid porous magnetic bentonite-chitosan beads for selective removal of radioactive cesium in water. *J Hazard Mater* 362: 160–169.
- WANG Q, RHIMI B, WANG H, WANG C. 2020. Efficient photocatalytic degradation of gaseous toluene over F-doped TiO₂/exfoliated bentonite. *Appl Surf Sci* 530: 147286.
- XU C, LU W, BIAN S, LIANG J, FAN Y, ZHANG X. 2012. Porous Collagen Scaffold Reinforced with Surface Activated PLLA Nanoparticles. *The Scientific World Journal*. Article ID 695137.
- XU X, CHENG Y, WU X, FAN P, SONG R. 2020. La(III)-bentonite/chitosan composite: a new type adsorbent for rapid removal of phosphate from water bodies. *Appl Clay Sci* 1901: Article 105547.